

Double-tag events study with the L3 detector at $\sqrt{s} = 189$ GeV

Pablo Achard ^a on behalf of the L3 Collaboration

^aUniversity of Geneva, DPNC, 24 quai E. Ansermet,
1211 Genève 4, Switzerland

A preliminary study of double tag events using the L3 detector at center of mass energy $\sqrt{s} \simeq 189$ GeV has been performed. The cross-section of $\gamma^*\gamma^*$ collisions is measured at average $\langle Q^2 \rangle = 14.5$ GeV². The results are in agreement with predictions based on perturbative QCD, while the Quark Parton Model alone is insufficient to describe the data. The measurements lie below the LO and above the NLO BFKL calculations.

1. Introduction

In this paper we present an update of the analysis of double-tag two-photon events: $e^+e^- \rightarrow e^+e^- \text{ hadrons}$ already published for $\sqrt{s} \simeq 91$ GeV and $\sqrt{s} \simeq 183$ GeV [1], obtained at LEP with the L3 detector. The data, collected at centre-of-mass energy $\sqrt{s} \simeq 189$ GeV, correspond to an integrated luminosity of 176 pb⁻¹. Both scattered electrons¹ are detected in the small angle electromagnetic calorimeters (Fig. 1). The virtuality of the two photons, Q_1^2 and Q_2^2 , is in the range of $3 \text{ GeV}^2 < Q_{1,2}^2 < 37 \text{ GeV}^2$. The centre-of-mass energy of the two virtual photons, $\sqrt{\hat{s}} = W_{\gamma\gamma}$, ranges from 3 GeV to 75 GeV.

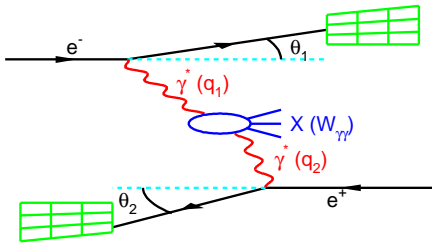


Figure 1. Kinematics of a double-tag event.

¹Electron stands for electron or positron throughout this paper.

For $Q_1^2 \approx Q_2^2 \approx 0$ (untagged events) [2], the two-photon cross-section, $\sigma_{\gamma\gamma}$, is dominated by vector-vector interactions, VDM (Fig. 2a).

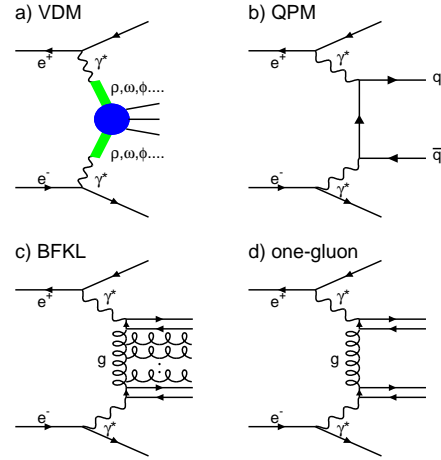


Figure 2. Diagrams for the a) VDM, b) QPM, c) BFKL Pomeron and d) one-gluon exchange processes in $\gamma^*\gamma^*$ interactions.

With increasing Q^2 , the VDM process is suppressed by the vector meson form factor and the Quark Parton Model process (QPM), shown in Fig. 2b, becomes important. Single-tag two-photon events, where $Q_1^2 \gg Q_2^2 \approx 0$, are usu-

ally analysed within the DIS formalism [3] and a photon structure function is introduced (*resolved photon*). Since the highly virtual photon, unlike the proton, does not contain constituent quarks with an unknown density distribution, one may hope to have a complete QCD calculation under particular kinematical conditions. In this formalism, used today by the Monte Carlo generators, one considers one or two resolved photons (*single or double resolved processes*) to calculate the QCD leading order diagrams.

An alternative QCD approach is based on the BFKL equation [4]. Here the highly virtual two-photon process, with $Q_1^2 \simeq Q_2^2$, is considered as the “golden” process where the calculation can be verified without phenomenological inputs [5,6]. The $\gamma^*\gamma^*$ interaction can be seen as the interaction of two $q\bar{q}$ pairs scattering off each other via multiple gluon exchange (Fig. 2c). For $\ln \hat{s}/Q^2 \approx 1$ a diagram with one-gluon exchange could be sufficient and the cross-section would be constant (Fig. 2d). In the limit of high energy, $\ln \hat{s}/Q^2 \gg 1$, the diagram of Fig. 2c is calculable by the resummation of the large logarithms. In this scheme the cross-section for the collision of two virtual photons is [5,6]:

$$\sigma_{\gamma^*\gamma^*} = \frac{\sigma_0}{\sqrt{Q_1^2 Q_2^2 Y}} \left(\frac{s}{s_0} \right)^{\alpha_P - 1}. \quad (1)$$

Here

$$\begin{aligned} \sigma_0 &= \text{const} \quad , \quad s_0 = \frac{\sqrt{Q_1^2 Q_2^2}}{y_1 y_2} \\ y_i &= 1 - (E_i/E_b) \cos^2(\theta_i/2) \end{aligned}$$

where E_b is the beam energy, E_i and θ_i are the energy and polar angle of the scattered electrons and α_P is the “hard Pomeron” intercept. The centre-of-mass energy of the two-photon system is related to the e^+e^- centre-of-mass energy s by $\hat{s} = W_{\gamma\gamma}^2 \approx s y_1 y_2$. In leading order one has $\alpha_P - 1 = (4 \ln 2) N_c \alpha_s / \pi$ where N_c is the number of colours. Using $N_c = 3$ and $\alpha_s = 0.2$, one obtains $\alpha_P - 1 \simeq 0.53$ [5,6]; in the next-to-leading order the BFKL contribution is calculated to be smaller, $\alpha_P - 1 \leq 0.17$ [7].

Double-tag interactions have been measured in previous experiments [8] at lower values of Q^2 and

$W_{\gamma\gamma}$. For comparison with the prediction of the BFKL models, the cross-sections will be given as a function of the variable $Y = \ln(s/s_0)$ instead of $W_{\gamma\gamma}$ as used in Ref. [2,8]. The advantage in using this variable is that Y is independent of the beam energy :

$$Y \approx \ln \left(\frac{(q_1 + q_2)^2}{\sqrt{q_1^2 q_2^2}} \right) \approx \ln \left(\frac{q_1^2 + 2q_1 \cdot q_2 + q_2^2}{q_1 q_2} \right)$$

with $q_{1,2}^2 = -2\sqrt{s} E_{tag1,2} (1 - \cos \theta_{1,2})$.
As $E_{tag1,2} \simeq \sqrt{s}/2$ and $m_e \simeq 0$:

$$Y \approx \ln \left(\frac{2 - \cos \theta_{\gamma_1 \gamma_2}}{2\sqrt{(1 - \cos \theta_1)(1 - \cos \theta_2)}} \right) \quad (2)$$

where $\theta_{\gamma_1 \gamma_2}$ is the angle between the two photons and $\theta_{1,2}$ are the tagging angles.

2. Monte Carlo Generators

The Monte Carlo generators used in this analysis are JAMVG [12] which generates events with the matrix element of Figure 2b and PHOJET [9] which gives a good description of the single-tag events [3] and uses the GRV-LO [11] parton density in the photon to initiate QCD processes.

The dominant backgrounds are $e^+e^- \rightarrow e^+e^-\tau^+\tau^-$, simulated by JAMVG [12], and single-tag two-photon hadronic events, where a hadron is misidentified as a scattered electron. The contamination by annihilation processes is simulated by PYTHIA [13] ($e^+e^- \rightarrow \text{hadrons}$), KORALZ [14] ($e^+e^- \rightarrow \tau^+\tau^-$) and KORALW [15] ($e^+e^- \rightarrow W^+W^-$).

All Monte Carlo events are passed through a full detector simulation using the GEANT [16] and the GEISHA [17] programs and are reconstructed in the same way as the data.

3. Data Analysis

3.1. Event Selection

A detailed description of the L3 detector is given in Ref. [18,19]. The two-photon hadronic events are mainly triggered by two independent triggers: the central track [20] and the single and double tag energy [21] triggers. The total trigger inefficiency of the selected events is less than 1%.

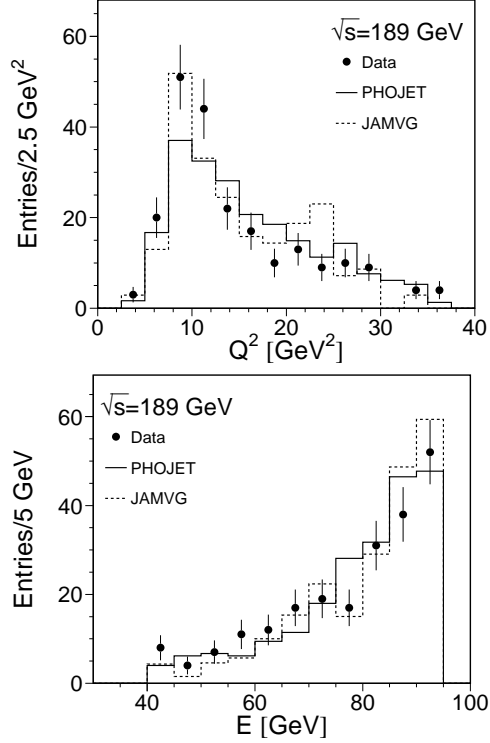


Figure 3. Distributions of Q^2 and energy of the scattered electrons. The data is compared to the Monte Carlo predictions, normalised to the number of data events. There are two entries per event.

Two-photon hadronic event candidates, $e^+e^- \rightarrow e^+e^- \text{hadrons}$, are selected using the following cuts:

- There must be two identified electrons, forward and backward (double-tag), in the small angle electromagnetic calorimeters. Each electron is identified as the highest energy cluster in one of the calorimeters, with energy greater than 40 GeV. The polar angle of the two tagged electrons has to be in the range $30 \text{ mrad} < \theta_1 < 66 \text{ mrad}$ and $30 \text{ mrad} < \pi - \theta_2 < 66 \text{ mrad}$.
- The number of tracks, measured in the polar angle region $20^\circ < \theta < 160^\circ$, must be greater than two. The tracks are required to have a transverse momentum, p_t , greater

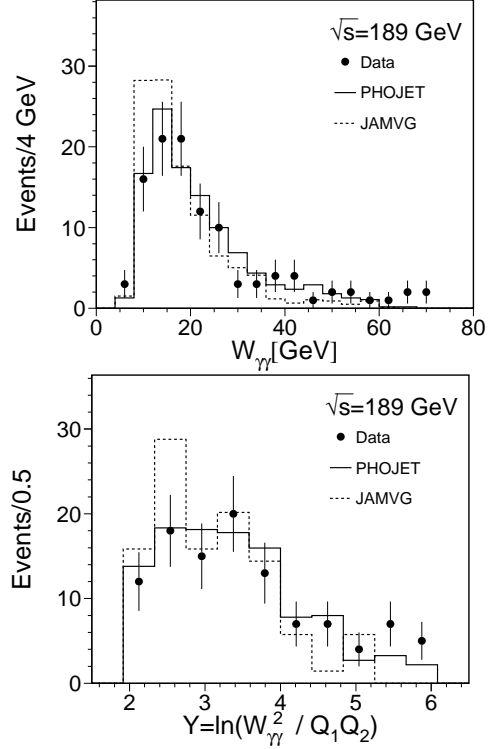


Figure 4. Distributions of the two-photon mass, $W_{\gamma\gamma}$, and the variable Y . The data are compared to the Monte Carlo predictions, normalised to the number of data events.

than 100 MeV and a distance of closest approach in the transverse plane to the interaction vertex smaller than 10 mm.

- The value of $Y = \ln(s/s_0)$ is required to be in the range $2 \leq Y \leq 6$.

After these cuts, 108 events are selected with an estimated background of 14 events from $e^+e^- \rightarrow e^+e^- \tau^+ \tau^-$ and misidentified single-tag events. The contamination from annihilation processes is negligible.

Contrary to the case of untagged or single-tag events the $W_{\gamma\gamma}$ measurement does not rely on the W_{vis} measurement. The analysis is, therefore, less dependent on the Monte Carlo modelling of the structure of the final state. The distributions of Q_i^2 and E_i of the two scattered electrons are shown in Fig. 3. In Fig. 4, the

Table 1

The differential cross-section, $d\sigma(e^+e^- \rightarrow e^+e^- \text{hadrons})/dY$ in picobarn measured in the kinematic region defined in the text, at $\sqrt{s} \simeq 189$ GeV. The predictions of the PHOJET and the JAMVG Monte Carlo are also listed. The first error is statistical and the second is systematic.

	DATA	PHOJET	DATA	JAMVG
	corrected with PHOJET		corrected with JAMVG	
ΔY	$d\sigma/dY$	$d\sigma/dY$	$d\sigma/dY$	$d\sigma/dY$
2 – 3	$0.39 \pm 0.06 \pm 0.06$	0.32	$0.39 \pm 0.07 \pm 0.06$	0.27
3 – 4	$0.24 \pm 0.04 \pm 0.04$	0.21	$0.22 \pm 0.04 \pm 0.03$	0.11
4 – 5	$0.11 \pm 0.03 \pm 0.02$	0.09	$0.08 \pm 0.02 \pm 0.01$	0.03
5 – 6	$0.08 \pm 0.03 \pm 0.01$	0.04	$0.07 \pm 0.02 \pm 0.01$	0.01

distributions of $W_{\gamma\gamma}$ and Y are presented. The variable $W_{\gamma\gamma}$ is calculated using the kinematics of the two scattered electrons, taking advantage of the good resolution of the energy of scattered electrons (about 1.3% [19]). The $W_{\gamma\gamma}$ resolution is about 18% at $W_{\gamma\gamma}/\sqrt{s} = 0.08$ and about 6% at $W_{\gamma\gamma}/\sqrt{s} = 0.2$. PHOJET gives a reasonable description of the shape of data. The absolute normalisation of PHOJET is about 20% too low.

3.2. Double-tag cross-section

The cross-sections are measured in the kinematic region limited by:

- $E_{1,2} > 30$ GeV, $30 \text{ mrad} < \theta_1 < 66 \text{ mrad}$ and $30 \text{ mrad} < \pi - \theta_2 < 66 \text{ mrad}$.
- $2 \leq Y \leq 6$.

The data are corrected for efficiency and acceptance with PHOJET. The correction factors vary from about 30% at low values of Y to about 80% at high values of Y . The correction factors calculated with JAMVG are similar. The differential cross-sections $d\sigma(e^+e^- \rightarrow e^+e^- \text{hadrons})/dY$ are measured in four ΔY intervals and are listed in Table 1.

The systematic error due to the selection cuts is 5%, estimated by varying the cuts. The uncertainty on the cross-section from the background estimation of single-tag events is 11%. The uncertainty due to the acceptance correction is 9%. The different systematic uncertainties are added in quadrature to give the total systematic error listed in Table 1.

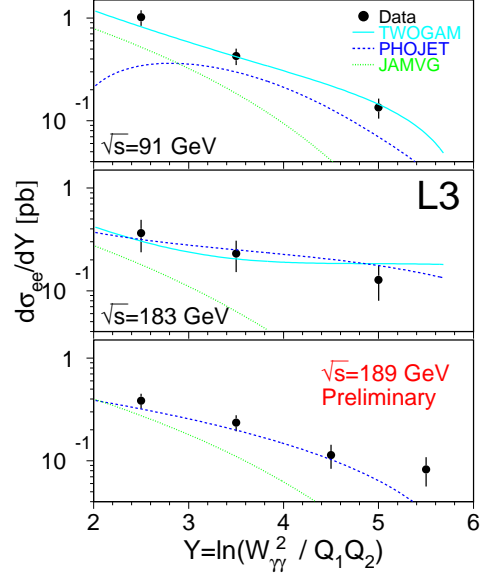


Figure 5. The cross-section of $e^+e^- \rightarrow e^+e^- \text{hadrons}$ as a function of Y in the kinematical region defined in the text at $\sqrt{s} \simeq 91, 183$ and 189 GeV compared to the predictions of the Monte Carlo models [9,10,12].

As can be seen in Table 1 and in Fig. 5, the data are in reasonable agreement with the predictions of the QCD Monte Carlo model implemented in PHOJET², whereas the QPM cross-section esti-

²The poor agreement at low Y for $\sqrt{s} = 91$ GeV is well understood (suppression of direct contribution due to a

mated with JAMVG, is not sufficient to describe the data.

From the measurement of the $e^+e^- \rightarrow e^+e^- \text{hadrons}$ cross-section, σ_{ee} , we extract the two-photon cross-section, $\sigma_{\gamma^*\gamma^*}$, by using only the transverse photon luminosity function [22,23], $\sigma_{ee} = L_{TT} \cdot \sigma_{\gamma^*\gamma^*}$. This measurement gives an effective cross-section containing contributions from transverse (T) and longitudinal (L) photon polarisations:

$$\sigma_{\gamma^*\gamma^*} = \sigma_{TT} + \epsilon_1 \sigma_{TL} + \epsilon_2 \sigma_{LT} + \epsilon_1 \epsilon_2 \sigma_{LL} \quad (3)$$

$$\epsilon_i = \frac{L_L}{L_T} = \frac{2(1 - y_i)}{1 + (1 - y_i)^2}$$

where ϵ_i is the ratio of transverse and longitudinal photon luminosity functions. In the present kinematical region the values of ϵ_i are greater than 0.97, but the values of σ_{TL} , σ_{LT} and σ_{LL} are expected to be small [5].

Table 2

The two-photon cross-section, $\sigma_{\gamma^*\gamma^*}$ in nanobarn without and after subtraction of the QPM contribution, as a function of Y at $\sqrt{s} \simeq 189$ GeV. The first error is statistical and the second is systematic.

ΔY	$\sigma_{\gamma^*\gamma^*}^{TOT}$	$\sigma_{\gamma^*\gamma^*}^{TOT-QPM}$
2 – 3	$7.5 \pm 1.3 \pm 1.1$	$2.2 \pm 0.4 \pm 0.3$
3 – 4	$7.3 \pm 1.3 \pm 1.1$	$3.8 \pm 0.6 \pm 0.6$
4 – 5	$5.5 \pm 1.5 \pm 0.8$	$4.2 \pm 1.1 \pm 0.6$
5 – 6	$7.4 \pm 2.3 \pm 1.1$	$6.7 \pm 2.1 \pm 1.0$

In Fig. 6 we show $\sigma_{\gamma^*\gamma^*}$, after subtraction of the QPM contribution given in Table 2, as a function of Y . Using an average value of Q^2 , $\langle Q^2 \rangle = 14.5 \text{ GeV}^2$, we calculate the one-gluon exchange contribution with the asymptotic formula (Eq. 10.2 of Ref. [5]). The expectations are below the data. The leading order expectations of the BFKL model (Eq. 4.19 of Ref. [5]), shown as a dotted line in Fig. 6, are too high. By leaving

too sever p_T cut)

α_P as a free parameter, a fit to the data, taking into account the statistical errors, yields:

$$\alpha_P - 1 = 0.29 \pm 0.03 \quad (4)$$

The results are shown in Fig. 6 as a continuous line. In the same figure are also shown our previous results [1] obtained at $\sqrt{s} \simeq 91$ GeV and $\sqrt{s} \simeq 183$ GeV. A combined fit of the three sets of data leaving α_P as a free parameter gives:

$$\alpha_P - 1 = 0.29 \pm 0.025 \quad (5)$$

with $\chi^2/d.o.f. = 7/10$ ($C.L. = 0.73$).

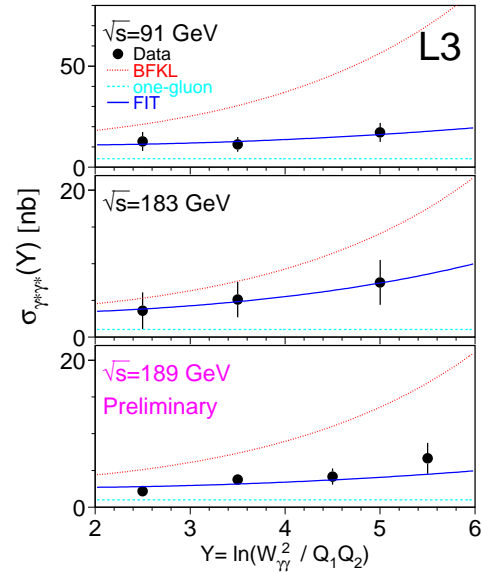


Figure 6. Two-photon cross-sections, $\sigma_{\gamma^*\gamma^*}$, after subtraction of the QPM contribution at $\sqrt{s} \simeq 91$ GeV ($\langle Q^2 \rangle = 3.5 \text{ GeV}^2$), $\sqrt{s} \simeq 183$ GeV ($\langle Q^2 \rangle = 14 \text{ GeV}^2$) and $\sqrt{s} \simeq 189$ GeV ($\langle Q^2 \rangle = 14.5 \text{ GeV}^2$). The data are compared to the predictions of the LO BFKL calculation and of the one-gluon exchange diagram. The continuous line is a fit to the data with Eq. 1 by leaving α_P as a free parameter.

But if one fixes α_P to its LO and NLO calculated values, one finds respectively:

$$\chi^2_{LO-BFKL}/d.o.f. = 263/10 \quad (C.L. < 10^{-16})$$

$$\chi^2_{NLO-BFKL}/d.o.f. = 21/10 \quad (C.L. = 0.021).$$

4. Conclusions

The cross-sections of double-tag $e^+e^- \rightarrow e^+e^- \text{hadrons}$ events is measured at $\sqrt{s} \simeq 189$ GeV. The events are well described by the PHOJET Monte Carlo model which uses the GRV-LO parton density in the photon and leading order perturbative QCD. A combined fit of our results obtained at $\sqrt{s} \simeq 91, 183$ and 189 GeV gives a value of $\alpha_P - 1$ smaller than expected from the LO BFKL calculations and higher than the value predicted by NLO BFKL calculations.

Acknowledgements

I would really like to thank Maneesh Wadhwa for providing me the results and some help, and all the L3 $\gamma\gamma$ group for discussions and support. Thanks also to the organizers of this interesting conference.

REFERENCES

1. L3 Collab., M. Acciarri *et al.*, Phys. Lett. B **453** (1999) 333-341
2. L3 Coll., M. Acciarri *et al.*, Phys. Lett. B **408** (1997) 450
3. L3 Coll., M. Acciarri *et al.*, Phys. Lett. B **436** (1998) 403;
L3 Coll., M. Acciarri *et al.*, Preprint CERN-EP/98-168, Phys. Lett. B accepted
4. E.A. Kuraev, L.N. Lipatov and V.S. Fadin, Sov. Phys. JETP **45** (1977) 199;
Ya.Ya. Balitski and L.N. Lipatov, Sov. J. Nucl. Phys. **28** (1978) 822
5. S.J. Brodsky, F. Hautmann and D.E. Soper, Phys. Rev. D **56** (1997) 6957
6. J. Bartels, A. De Roeck and H. Lotter, Phys. Lett. B **389** (1996) 742;
J. Bartels, A. De Roeck, C. Ewerz and H. Lotter, hep-ph/9710500
7. S.J. Brodsky, V.S. Fadin, V.T. Kim, L.N. Lipatov and G.B. Pivovarov, hep-ph/99101229
8. PLUTO Coll., C. Berger *et al.*, Phys. Lett. B **142** (1984) 119;
TPC/2 γ Coll., D. Bintinger *et al.*, Phys. Rev. Lett. **54** (1985) 763;
MD-1 Coll., S.E. Baru *et al.*, Z. Phys. C **53** (1992) 219;
TOPAZ Coll., R. Enomoto *et al.*, Phys. Lett. B **368** (1996) 299
9. PHOJET version 1.05c is used.
R. Engel, Z. Phys. C **66** (1995) 203;
R. Engel and J. Ranft, Phys. Rev. D **54** (1996) 4244
10. TWOGAM version 1.71 is used.
L. Lönnblad *et al.*, “ $\gamma\gamma$ event generators”, in Physics at LEP2, ed. G. Altarelli, T. Sjöstrand and F. Zwirner, CERN 96-01 (1996), Volume 2, 224.
S. Nova *et al.*, DELPHI Note 90-35 (1990).
We thank our colleagues from DELPHI to make their program available to us
11. M. Glück, E. Reya and A. Vogt, Phys. Rev. D **45** (1992) 3986;
M. Glück, E. Reya and A. Vogt, Phys. Rev. D **46** (1992) 1973
12. J.A.M. Vermaseren, Nucl. Phys. B **229** (1983) 347
13. T. Sjöstrand, Comp. Phys. Comm. **82** (1994) 74
14. S. Jadach, B.F.L. Ward and Z. Wąs, Comp. Phys. Comm. **79** (1994) 503
15. M. Skrzypek, S. Jadach, W. Placzek and Z. Wąs, Comp. Phys. Comm. **94** (1996) 216;
M. Skrzypek, S. Jadach, M. Martinez, W. Placzek and Z. Wąs, Phys. Lett. B **372** (1996) 289
16. R. Brun *et al.*, GEANT 3.15 preprint CERN DD/EE/84-1 (Revised 1987)
17. H. Fesefeldt, RWTH Aachen report PITHA 85/2 (1985)
18. L3 Collab., B. Adeva *et al.*, Nucl. Inst. Meth. A **289** (1990) 35
19. I.C. Brock *et al.*, Nucl. Inst. Meth. A **381** (1996) 236
20. P. Béné *et al.*, Nucl. Inst. Meth. A **306** (1991) 150
21. R. Bizzarri *et al.*, Nucl. Inst. Meth. A **283** (1989) 799
22. V.M. Budnev *et al.*, Phys. Rep. C **15** (1975) 181
23. G.A. Schuler, Comput. Phys. Commun. **108** (1998) 279